Saudi Journal of Biological Sciences 28 (2021) 1233–1238

Contents lists available at ScienceDirect

Saudi Journal of Biological Sciences

journal homepage: www.sciencedirect.com

Original article

Manganese-doped cerium oxide nanocomposite as a therapeutic agent for MCF-7 adenocarcinoma cell line

M. Atif [a], Seemab Iqbal [b,*], M. Fakhar-e-Alam [b,*], Qaisar Mansoor [c], K.S. Alimgeer [d], Amanullah Fatehmulla [a], Atif Hanif [e], Nafeesah Yaqub [a], W.A. Farooq [a], Shafiq Ahmad [f], Hijaz Ahmad [g,h], Yu-ming Chu [i,j,*]

[a] Department of Physics and Astronomy, College of Science, King Saud University, Riyadh 11451, Saudi Arabia
[b] Department of Physics, GC University, Faisalabad 38000 Pakistan
[c] Institute of Biomedical and Genetic Engineering, Islamabad, Pakistan
[d] Department of Electrical and Computer Engineering, COMSATS University, Islamabad, Islamabad campus, Pakistan
[e] Botany and Microbiology Department, College of Science, King Saud University, Riyadh 11451, Saudi Arabia
[f] Industrial Engineering Department, College of Engineering, King Saud University, P.O. Box 800, Riyadh 11421, Saudi Arabia
[g] Department of Basic Sciences, University of Engineering and Technology, Peshawar 25000, Pakistan
[h] Section of Mathematics, International Telematic University Uninettuno, Corso Vittorio Emanuele II, 39, 00186 Roma, Italy
[i] Department of Mathematics, Huzhou University, Huzhou 313000, China
[j] Hunan Provincial Key Laboratory of Mathematical Modeling and Analysis in Engineering, Changasha, University of Science & Technology, Changsha 410114, China

ARTICLE INFO

Article history:
Received 13 November 2020
Revised 5 December 2020
Accepted 6 December 2020
Available online 11 December 2020

Keywords:
$Mn:CeO_2$ nanocomposite
XRD
SEM
MCF-7 adenocarcinoma cell line
Cytotoxicity
Mathematical modeling
Cancer therapy

ABSTRACT

The preparation of a manganese-doped cerium oxide ($Mn:CeO_2$) nanocomposite via hydrothermal route is described. Cubic fluorite structure of single phase was exhibited by studying structural analysis through x-ray diffraction (XRD) technique and morphological analysis was conducted by scanning electron microscope. Surface analytic technique of energy dispersive x-ray spectroscopy (EDX) was conducted to analyze the relative amount of any impurity and doping. Structural changes due to manganese doping such as increment in production of vacancies of oxygen within crystal of cerium oxide, and reduction in size of crystallite and constant of lattice was observed in our research study. Moreover, the $Mn:CeO_2$ nanocomposite demonstrates differential cytotoxicity against MCF-7 adenocarcinoma cell line, which renders it a promising candidate for targeted cancer therapy. The anti-tumorous activity of the cerium oxide nanocomposite was significantly enhanced with doping of manganese, which is directly linked with the generation of highly reactive oxygen facets. The experimental results are supported by a mathematical model that confirms a confidence level of 95%. This research has paved the way for many utilities in therapeutics and magnetic resonance imaging diagnostics through new observations, and hence verified their math model.

1. Introduction

The cytotoxicity of metallic nanoparticles (NPs) is known to be enhanced by doping with other materials (Wojcieszak et al., 2018). Doping often results in an enhancement of the production of reactive oxygen species (ROS), which renders these nanoscale particles associated with metals or metal oxides good candidates for treatment of different cancer and bacterial diseases (Luo et al., 2018).

Cerium oxide (CeO_2), also called ceria, is an insulating and ionic oxide with a cubic fluorite-like structure (CaF_2) containing Ce^{3+} and Ce^{4+} ions. Although ceria itself has no particular biological significance (Kumar et al., 2013); its nanoparticles having the ionic form Ce^{3+} are relevant biocompatible ingredients of antiemetic, bacteriostatic, bactericidal, and antitumor agents (Abbas et al., 2015). In addition, due to their ionic behavior, these NPs are suitable for treatment of fetal diseases like cancer, and their ROS activities have been recently a research target (Saranya et al., 2014). The biological properties of these NPs, including biodistribution, toxicity, elimination, and dissolution, depend on their physical and chemical characteristics.

* Corresponding authors.
E-mail addresses: seemabiqbal11@hotmail.com (S. Iqbal), fakharphy@gmail.com (M. Fakhar-e-Alam), chuyuming2005@126.com (Y.-m. Chu).
Peer review under responsibility of King Saud University.

Production and hosting by Elsevier

https://doi.org/10.1016/j.sjbs.2020.12.006
1319-562X/

CeO_2 also exhibits catalytic properties that stem from its redox properties, structural defects such as high reactive oxygen species and their harmful effects during catalytic process (Asati et al., 2010). These catalytic properties, as well as the oxygen reserve and transfer capacity of CeO_2, can be enhanced by doping, which has led to the development of biomedical applications (Chaudhari et al., 2017).

Manganese, which has an abundance of 0.1% and is one of the 12 most occurring metals in the earth crust, is one of the most promising dopants for CeO_2 NPs because its ionic radius is similar to that of Ce (Parvathya and Venkatramanb, 2017). An essential nutrient for animals and plants with a key role in bone formation and the urea cycle, Mn is usually found in nature forming oxides, carbonates, and silicates in more than 100 minerals. Its wound hailing ability has attracted the attention of researchers, and its toxicological properties, along with that of other metallic nanoparticles, is a hot research topic.

For cancer treatment, ROS production in malignant cells is actively investigated as one of the major factors for destruction of infected cells. This production of ROS is highly dependent on defects states in cells. In CeO_2 NPs, defects may be generated by Mn doping; therefore, this can be envisaged as an effective approach to enhance the anticancer activity in cells (Ansari et al., 2016). Herein, CeO_2 NPs are doped with Mn to examine its toxicological effects (Celardo et al., 2011). Considering the need for a cost effective and environment friendly preparation method that allows morphology control (Jayakumar et al., 2017), the present Mn-doped CeO_2 nanocomposites are prepared via hydrothermal approach, which is safe, can be conducted at room temperature, and enables NP size control by controlling the pH. The successful growth and structure of these nanoparticles is confirmed by diffraction technique: XRD and electronic microscopic scan: SEM. The bacterial and photodynamic effects on an MCF-7 adenocarcinoma cell line are investigated. A schematic illustration of the preparation process is shown in Fig. 1.

2. Materials and methods

2.1. Chemical and reagents

Cerium (III) nitrate hexahydrate ($Ce(NO_3)_2{\cdot}6H_2O$; 432.2 g/mole; 99.9% purity), manganese chloride ($MnCl_2{\cdot}4H_2O$), sodium hydroxide (NaOH; 40 g/mole; 99.9% purity), and acetic acid (CH_3COOH) were procured from Sigma-Aldrich Chemicals. Double distilled water was used as solvent to prepare the solutions. In all the experimental work, acid washed glassware was used.

2.2. Hydrothermal synthesis of manganese-doped cerium oxide nanoparticles

Mn-doped CeO_2 NPs were synthesized by hydrothermal method using $MnCl_2{\cdot}4H_2O$ and $Ce(NO_3)_2{\cdot}6H_2O$ as precursors. In a typical procedure, a 1 M solution of $Ce(NO_3)_2{\cdot}6H_2O$ in 100 mL of deionized water was mixed with a 7 M solution of $MnCl_2{\cdot}4H_2O$ under constant magnetic stirring with a speed of 7000–10000 rpm. Then, 2 mL of acetic acid was poured drop by drop into the solution as a capping agent to control/minimize the particle size of the nanocomposite, and a basic solution of 1 M (8 g/100 mL) NaOH was slowly added under constant stirring to attain a pH of 10. After 1–2 h, a brownish white colloidal solution was obtained. Then, the colloid was separated by centrifugation, and the precipitate was placed in a water bath at 75 °C for 20–30 min. The collected sample was shifted to the Teflon auto-clave. The dried sample was then calcined in an electric furnace at 600 °C for 4–6 h to obtain the final NPs, which were subjected to XRD analysis (Jayakumar et al., 2017; Syed Khadar et al., 2019).

2.3. Anticancer activity and cytotoxicity analysis

The percent cell viability and anticancer activity of the Mn: CeO_2 nanocomposite in the absence or presence of 5-ALA drug was assessed for MCF-7 breast cancer cell line through colorimetric assay for assessing cell metabolic activity. For this experiment, the chosen cell line was collected at an oncology lab of a tertiary care hospital in Islamabad. Cytotoxicity and analysis of generation of reactive oxygen species: ROS analysis of the manufactured nanocomposites toward these tumorous cells were performed through our published protocol in reported articles (Atif et al., 2019; Ahamed et al., 2016; Mehmood Ur Rehman et al., 2017). Cells were grown in RPMI complemented with 10% fetal calf serum (FCS) and 5% GPPS antibiotics in a 75 cm^3 culture flask at 37 °C in the presence of 5% CO_2 in a SHELLAB incubator. The cell lines were grown in a cultural plate:96-well plate having proportion of 10^5 cells per well. The cells were admitted to stick to the surficial wall for 48 h by incubating them at 37 °C and 5% CO_2 for one day. After which, the cells were treated with Mn:CeO_2 nanocomposite (20 g/mL) for one day. The suspensions of the Mn:CeO_2 nanocomposite were poured to the cells. Cells in absence of nanocomposite were taken as control in this conducted study. They were poured into the cultural plates at a concentration of 10^6 cells/well along with various concentrations of Mn: CeO_2 nanocomposite and further incubated for a day. Briefly, 10 μL MTT (5 mg/mL) was poured to the wells for determining viability of the cells. The cultural plate was further put in the incubator for 2–3 h under the same incubation conditions. Afterwards, a solubilization process, the

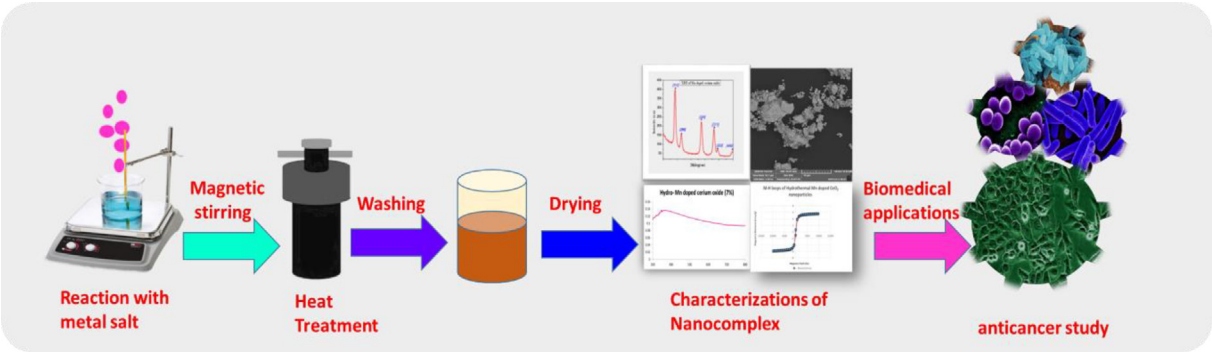

Fig. 1. Schematic illustration of the preparation process.

absorbance was recorded at 550 nm using a PLATOS R 496 plate reader (Atif et al., 2019; Iqbal et al., 2015).

Formulation of viable cells was measured by:

$$\text{Percentage of viable cells} = \frac{\text{Absorbance of the nanocomposite sample} - \text{Absorbance of the Blank}}{\text{Absorbance of } -\text{ve control} - \text{Absorbance of Blank}} \times 100$$

2.4. Characterization

The crystallographic study of the manufactured nanocomposite was condcuted by using a D8 Advance X-ray diffractometer (Bruker AXS) using monochromatic Cu Kα rays having 2 θ speed of scan per minute. The dimensions (size) and surficial study was measured and analyzed by SEM (Tescan Vega 3 LMU SEM). The absorbance of the bacterial cultures was observed using a nanodrop Thermo 2000 °C spectrophotometer (Thermo Fisher Scientific, USA) with a peak analyzer system. A Platos R 496 microplate reader (Ameda Labor diagnostik GmbH, Graz, Austria) was used to measure the absorbance of the MTT-treated cell line at 550 nm.

3. Results

3.1. Structural study

Typical XRD patterns of the Mn: CeO_2 sample calcined at 600 °C are depicted in Fig. 2. The obtained 2θ values of 28.6°, 33.0°, 47.5°, 56.4°, 59.3°, and 69.5° are attributable to the (111), (200), (220), (311), (222), and (400) planes, respectively, similarly as described in previous reports (Saikia et al., 2017). The ionic radius of Ce^{4+} (1.03 Å) is larger than that of Mn^{2+} (0.74 Å) and, therefore, the latter ions can substitute the former in the CeO_2 crystal lattice. The crystallographic variables, i.e., D; size of the crystallite and constants of lattice (a = b = c) were measured using the given formulation:

$$D = \frac{0.89\lambda}{\beta\cos\theta} \quad and \quad d = \frac{a = b = c}{\sqrt{h^2 + k^2 + l^2}}$$

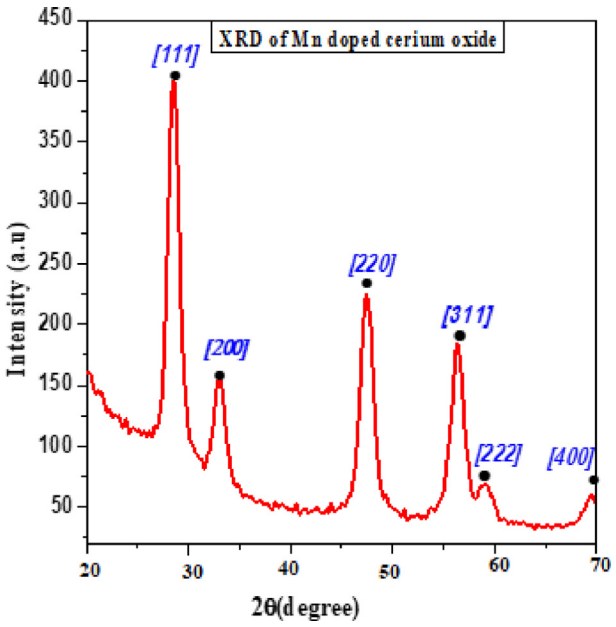

Fig. 2. Structural analysis of the Mn:CeO_2 nanocomposite prepared via hydrothermal method.

where β is the FWHM; full width at half maximum in radians, and h, k, and l represent the indices of Miller. Calculated D (size of crystallite) was 59.44 nm for the Mn: CeO_2 nanocomposite sample from the Scherrer formulations as given above.

3.2. Morphology analysis and energy dispersive X-Ray (EDX) analysis

The study of anatomies of the manufactured nanocomposite were analyzed by SEM. Fig. 3(a) depicts the structural anatomy of the Mn: CeO_2 sample. The SEM micrographs clearly reveal the spherical structure in nano-range, which appeared to have homogeneous distribution of shape and size of the particle. The calculated mean size of the grain was average NPs 105 nm.

EDX spectroscopy is generally used to determine the presence of incorporated specific elements/dopant and their corresponding percentages into the samples. The EDX graph of Fig. 3(b) shows one extra peak in agreement with the chlorine from $MnCl_2$, corresponding with the calculated and observed crystallographic data.

3.3. Cytotoxic analysis

The cytotoxicity of the prepared Mn:CeO_2 nanocomposites was examined for MCF-7 breast tumorous cell line as shown in Fig. 4. The cell line was incubated with 20 mg/mL solutions of the manufactured Mn:CeO_2 nanocomposites for a day.

The in-vitro analysis on cells of human breast cancer cells and math model simulations have revealed that average NPs 105 nm are translocated proficiently within surficial tissue resulting in harming the structure of cell including strong cellular uptake (Gustafson et al., 2015) with no toxicity is shown in Fig. 5.

3.4. Mathematical analysis

The data was collected using different experiments for different values of ppm NP for each DMEM (Dulbecco's Modified Eagle's medium) and Mn-doped CeO_2. The results presented were used for mathematical modeling and curve fitting presented in Fig. 6.

4. Discussion

The XRD patterns, which are coincident with typical values of CeO_2 (JCPDS card no. 43-1002), clearly indicate the formation of a face-centered cubic fluorite structure (Anupriya et al., 2014). The absence of MnO or any other impurity phases reveals the phase purity of the prepared samples and suggests the possible substitution of Mn ions on the Ce sites. Hence, the peak broadening increased due to the decreased particle size, as shown in Fig. 2 (Abbas et al., 2016).

Generally, metal ion doping at optimal level hinders the particle growth. The effect of Mn doping on the size reduction of the CeO_2 nanocomposite can be attributed to grain-boundary pinning affected by dopant ions, which bounds the grain growth by symmetry-breaking effects of the dopant at the boundary, resulting in particles with smaller size. The reduction in NP size after doping has been previously reported (Kumar et al., 2013; Jayakumar et al., 2017). SEM image reveals the cluster formation mechanism with crystal growth. This crystal growth is also confirmed by XRD. The analysis behind the crystal growth in the

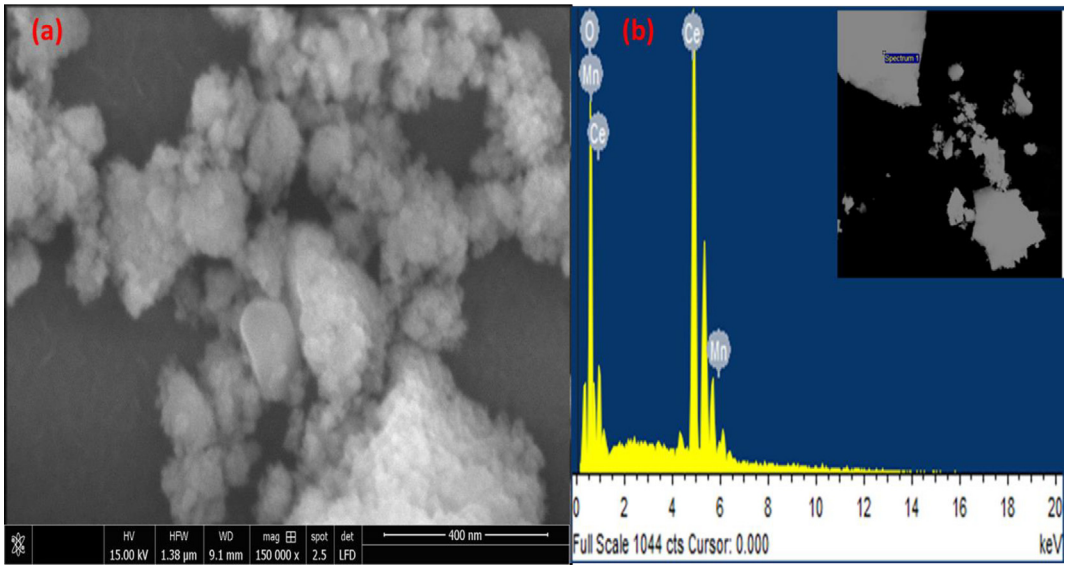

Fig. 3. (a) Morphological and (b) energy dispersive X-ray spectroscopy analysis of the Mn:CeO_2 nanocomposite.

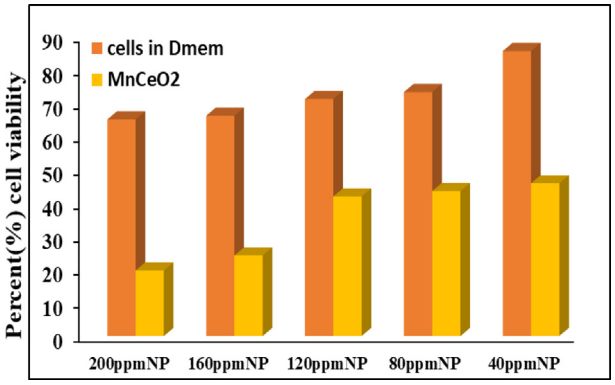

Fig. 4. Cytotoxicity of the Mn:CeO_2 nanocomposite in MCF-7 cancer cell line.

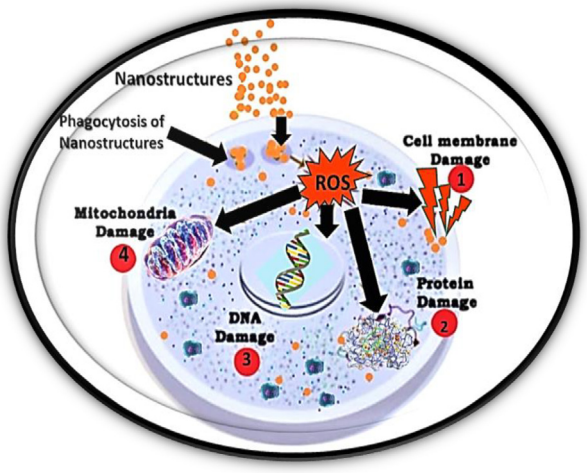

Fig. 5. Mechanism of the interaction of nanostructures with cancerous cells.

morphology of ceria is discussed by the previous reported studies explaining two common mechanisms called Ostwald ripening (OR), and Oriented attachment (OA) (Wu et al., 2008; Lin et al., 2012).

Furthermore, the EDX plot strongly coincident with the typical peak positions of La, Fe, Mn, and O. Ce was also identified by EDX spectroscopy because the energy of Mn (5.88) is very adjacent to that of Ce (6.02) (Abbas et al., 2016).

Synthesized Mn-doped CeO_2 nanocomposite anticancer activity was considerably greater in comparisons to other metal oxide nanostructures. For instance, Alhadlaq et al. reported in 2015 the cytotoxicity and oxidative stress of zinc ferrite in HepG2, A431, and A549 (Alhadlaq et al., 2015); Watanabe et al. discussed in 2013 the inhibition of A549 cancerous cells using Fe_3O_4 magnetic NPs (Watanabe et al., 2013); Alarifi et al. reported in 2014 a 16% inhibition in the % cellular viability of MCF-7 cancerous cells by Fe_2O_3 nanoparticles (Alarifi et al., 2014). In our case, 68% viability was inhibited using 200 ppm of a NP suspension of the Mn:CeO_2 nanocomposite, as shown in Fig. 4.

The highly selective cytotoxic performance of the synthesized Mn:CeO_2 nanocomposite may be of high clinical important because conventional anticancer drugs are often not able to discriminate between healthy and cancerous cells (Abbas et al., 2017). The nanomaterials toxicity is dependent on numerous factors such as composition and type of the nanomaterials, shape, particle size, and surface area, crystallinity, and solubility (Atif et al., 2019; Ahamed et al., 2016; Mehmood Ur Rehman et al., 2017; Mehmood Ur Rehman et al., 2018; Mehmood Ur Rehman et al., 2019). An elevated oxidative stress can be proposed as the main reason for the decrease of cell viability in the present study. Moreover, as can be extracted from Fig. 4, Mn-doped CeO_2 nanocomposites produced considerably higher amount of ROS in the MCF-7 cell line. This enhancement in ROS production has been previously related with the oxygen vacancies. Thus, the presence of structural defects (oxygen vacancies) in the crystal structure of Mn-doped metal oxides nanostructures leads to increased ROS generation (Abbas et al., 2015; Abbas et al., 2015; Iqbal et al., 2019). We previously observed a similar relation for Fe-doped CeO_2; however, no such a connection has been found in the case of Co-doped CeO_2 NPs (Iqbal et al., 2019; Iqbal et al., 2019). Hence, further investigation is needed.

The membrane integrity is disrupted by positively charged NPs and their toxicity is high as compared to negatively charged NPs (Anupriya et al., 2014) due to their low toxicity toward eukaryotic cells. Their easy surface modifications and biocompatibility is shown in Fig. 5. In short, Mn-doped CeO_2 nanocomposites are

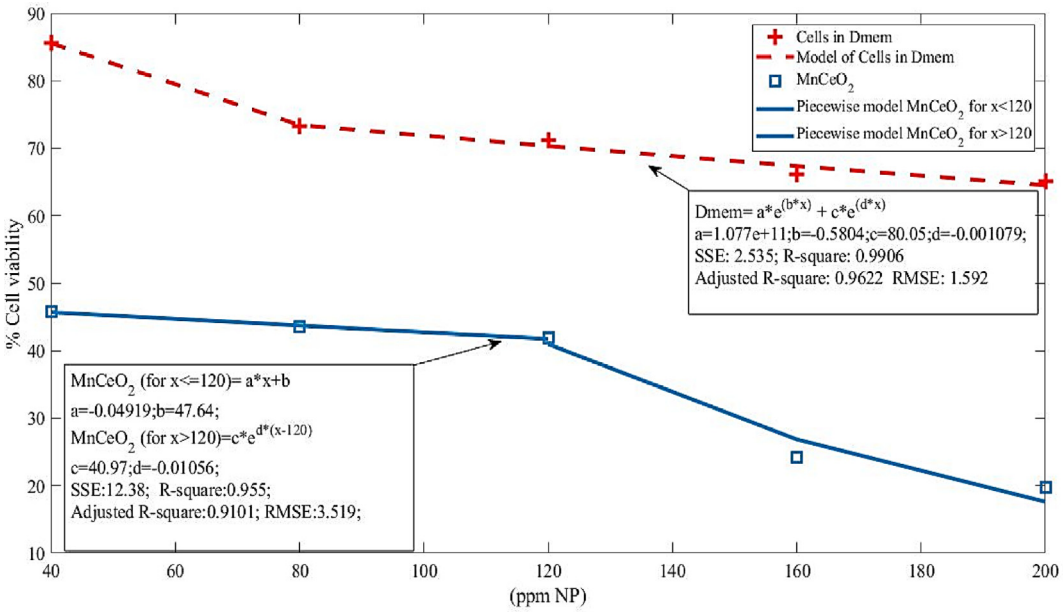

Fig. 6. % Cell viability for MCF-7 cell line of hydrothermally synthesized Mn-doped cerium oxide nanocomposites.

promising candidates for biosensor applications, drug delivery, and biomedical imaging including bacterial detection and antibacterial activity (Abbas et al., 2016).

The least-square error method was used to model the data for identifying the best possible values of the constants for the linear and exponential models presented in Fig. 6.

The reason for the selection of a biexponential model for DMEM is the nature of the decaying % cell viability with the increase in ppm NP. It can be observed that the fitted model is close to the data points and hence satisfies the 95% confidence level. The values for the constants used in mathematical modeling, which were extracted using Matlab software, are presented in Fig. 6, along with the values of goodness of fit for DMEM. It can be observed that the values of goodness of fit were satisfactory (Fakhar-e-Alam et al., 2020).

Similarly, the data for Mn-doped CeO_2 were also modeled using least-square errors; however, unfortunately, lower level of confidence was obtained because only a polynomial function was found to fit the data. Therefore, data were divided into two discontinuous functions (Iqbal et al., 2019) depending on the nature of the data. The first few data points followed a straight line, and a linear model was adopted as the curve-fitting tool. Then, the later portion followed a decaying exponential trend, and hence an exponential model was selected to fit the data. The values of the constants for both functions and a reasonable goodness of fit are included in Fig. 6 (Atif et al., 2020).

5. Conclusions

Mn-doped CeO_2 nanocomposites are found to be promising candidates for drug delivery and anticancer therapy. An $Mn_xCe_{1-x}O_2$ nanocomposite was successfully synthesized by hydrothermal method. Microstructural characterization by XRD, SEM, and EDX verified its morphology as cubic fluorite phase, nanospherical shape, and doping composition. The Mn-doped CeO_2 nanocomposite showed significant cytotoxic activity, demonstrating a 68% growth reduction of MCF-7 cancerous cells upon Mn doping most likely due to generation of oxygen vacancies resulting from ROS production. The experimental results were verified by mathematical modeling generated by applying the least-square error method using Matlab, which yielded a 95% confidence level.

Declaration of Competing Interest

The authors declare that they have no known competing financial interests or personal relationships that could have appeared to influence the work reported in this paper.

Acknowledgments

The authors extend their appreciation to the Deanship of Scientific Research at King Saud University for funding this work through research group number RGP-293. The author would like to specially thank the Higher Education Commission (HEC) Pakistan for the financial support under NRPU Grant No. 8056/Punjab/NRPU/R&D/HEC/ 2017. The research was supported by the National Natural Science Foundation of China (Grant Nos. 11971142, 11871202, 61673169, 11701176, 11626101, 11601485).

References

Abbas, F., Jan, T., Iqbal, J., Ahmad, I., Naqvi, M.S.H., Malik, M., 2015. Facile synthesis of ferromagnetic Ni doped CeO_2 nanoparticles with enhanced anticancer activity. Appl. Surf. Sci. 357, 931–936. https://doi.org/10.1016/j.apsusc.2015.08.229.

Abbas, F., Iqbal, J., Jan, T., Naqvi, M.S.H., Gul, A., Abbasi, R., et al., 2015. Differential cytotoxicity of ferromagnetic Co doped CeO_2 nanoparticles against human neuroblastoma cancer cells. J. Alloys Compd. 648, 1060–1066. https://doi.org/10.1016/j.jallcom.2015.06.195.

Abbas, F., Jan, T., Iqbal, J., Naqvi, M.S.H., 2015. Fe doping induced enhancement in room temperature ferromagnetism and selective cytotoxicity of CeO_2 nanoparticles. Curr. Appl. Phys. 15, 1428–1434. https://doi.org/10.1016/j.cap.2015.08.007.

Abbas, F., Iqbal, J., Jan, T., Badshah, N., Mansoor, Q., Ismail, M., et al., 2016. Structural, morphological, Raman, optical, magnetic, and antibacterial characteristics of CeO_2 nanostructures. Int. J. Miner. Metall. Mater. 23, 102–108. https://doi.org/10.1007/s12613-016-1216-1.

Abbas, F., Jan, T., Iqbal, J., Naqvi, M.S.H., Ahmad, I., 2016. Inhibition of neuroblastoma cancer cells viability by ferromagnetic mn doped CeO_2 monodisperse nanoparticles mediated through reactive oxygen species. Mater. Chem. Phys. 173, 1–6. https://doi.org/10.1016/j.matchemphys.2016.01.042.

Abbas, F., Iqbal, J., Maqbool, Q., Jan, T., Ullah, M.O., 2017. ROS mediated malignancy cure performance of morphological, optical, and electrically tuned Sn doped CeO_2 nanostructures. A.I.P. Adv. 7, 1–11 http://www.ncbi.nlm.nih.gov/pubmed/095205.

Ahamed, M., Khan, M.A.M., Akhtar, M.J., Alhadlaq, H.A., Alshamsan, A., 2016. Role of Zn doping in oxidative stress mediated cytotoxicity of TiO 2 nanoparticles in human breast cancer MCF-7 cells. Sci. Rep. 6, 30196. https://doi.org/10.1038/srep30196.

Alarifi, S., Ali, D., Alkahtani, S., Alhader, M.S., 2014. Iron oxide nanoparticles induce oxidative stress, DNA damage, and caspase activation in the human breast cancer cell line. Biol. Trace Elem. Res. 159, 416–424. https://doi.org/10.1007/s12011-014-9972-0.

Alhadlaq, H.A., Akhtar, M.J., Ahamed, M., 2015. Zinc ferrite nanoparticle-induced cytotoxicity and oxidative stress in different human cells. Cell Biosci. 5, 55. https://doi.org/10.1186/s13578-015-0046-6.

Ansari, A.A., Labis, J.P., Alam, M., Ramay, S.M., Ahmad, N., Mahmood, A., 2016. Synthesis, structural and optical properties of mn-doped ceria nanoparticles: a promising catalytic material. Acta Metall. Sin. (Engl. Lett.) 29, 265–273. https://doi.org/10.1007/s40195-016-0387-0.

Anupriya, K., Vivek, E., Subramanian, B., 2014. Facile synthesis of ceria nanoparticles by precipitation route for UV blockers. J. Alloys Compd. 590, 406–410. https://doi.org/10.1016/j.jallcom.2013.12.121.

Asati, A., Santra, S., Kaittanis, C., Perez, J.M., 2010. Surface-charge-dependent cell localization and cytotoxicity of cerium oxide nanoparticle. A.C.S. Nano 4, 5321–5331. https://doi.org/10.1021/nn100816s.

Atif, M., Iqbal, S., Fakhar-E-Alam, M., Ismail, M., Mansoor, Q., Mughal, L., et al., 2019. Manganese-doped cerium oxide nanocomposite induced photodynamic therapy in MCF-7 cancer cells and antibacterial activity. BioMed Res. Int. 2019, 1–13. https://doi.org/10.1155/2019/7156828.

Atif, M., Devanesan, S., AlSalhi, M.S., Masilamani, V., Saleem, M.N.A., AlShebly, M., et al., 2020. An experimental and algorithm-based study of the spectral features of breast cancer patients by a photodiagnosis approach. Photodiagn. Photodyn. Ther. 31,. https://doi.org/10.1016/j.pdpdt.2020.101851 101851.

Celardo, I., Pedersen, J.Z., Traversa, E., Ghibelli, L., 2011. Pharmacological potential of cerium oxide nanoparticles. Nanoscale 3, 1411–1420. https://doi.org/10.1039/c0nr00875c.

Chaudhari, S.P., Bodade, A.B., Jolhe, P.D., Meshram, S.P., Chaudhari, G.N., 2017. PEG-200 assisted sonochemical synthesis of cerium (Ce3+) doped copper oxide (CuO) nano-composites and their photocatalytic activities. Am. J. Mater. Synth. Process. 2, 97–102.

Fakhar-e-Alam, M., Aqrab-ul-Ahmad, Atif, M., Alimgeer, K. S., Suleman Rana, M., Yaqub, N., et al., 2020. Synergistic effect of TEMPO-coated TiO2 nanorods for PDT applications in MCF-7 cell line model. Saudi J. Biol. Sci. 27, 3199–3207. https://doi.org/10.1016/j.sjbs.2020.09.027.

Gustafson, H.H., Holt-Casper, D., Grainger, D.W., Ghandehari, H., 2015. Nanoparticle uptake: The phagocyte problem. Nano Today 10, 487–510. https://doi.org/10.1016/j.nantod.2015.06.006.

Iqbal, S., Fakhar-e-Alam, M., Akbar, F., Shafiq, M., Atif, M., Amin, N., et al., 2019. Application of silver oxide nanoparticles for the treatment of cancer. J. Mol. Struct. 1189, 203–209. https://doi.org/10.1016/j.molstruc.2019.04.041.

Iqbal, S., Fakhar-e-Alam, M., Amin, N., Ismail, M., Mustafa, G., Raza Ahmad, M., et al., 2019. Synthesis and study of structural, morphological, optical, and toxicological properties of ferromagnetic cobalt oxide nanoparticles in liver carcinoma cell line. Int. J. Mater. Res. 110, 481–483. https://doi.org/10.3139/146.111759.

Iqbal, S., Fakhar-e-Alam, M., Atif, M., Amin, N., Alimgeer, K.S., Ali, A., et al., 2019. Structural, morphological, antimicrobial, and in vitro photodynamic therapeutic assessments of novel Zn+ 2-substituted cobalt ferrite nanoparticles. Results Phys. 15. https://doi.org/10.1016/j.rinp.2019.102529.

Iqbal, S., Fakhar-e-Alam, M., Atif, M., Ahmed, N., Ul-Ahmad, A., Amin, N., et al., 2019. Empirical modeling of Zn/ZnO nanoparticles decorated/conjugated with fotolon (chlorine e6) based photodynamic therapy towards liver cancer treatment. Micromachines 10, 60. https://doi.org/10.3390/mi10010060.

Iqbal, J., Jan, T., Ul-Hassan, S.U., Ahmed, I., Mansoor, Q., Umair Ali, M., et al., 2015. Facile synthesis of Zn doped CuO hierarchical nanostructures: structural, optical and antibacterial properties. A.I.P. Adv. 5. https://doi.org/10.1063/1.4937907.

Jayakumar, G., Irudayaraj, A.A., Raj, A.D., 2017. Particle size effect on the properties of cerium oxide (CeO2) nanoparticles synthesized by hydrothermal method.

Kumar, E., Selvarajan, P., Muthuraj, D., 2013. Synthesis and characterization of CeO_2 nanocrystals by solvothermal route. Mat. Res. 16, 269–276. https://doi.org/10.1590/S1516-14392013005000021.

Lin, M., Fu, Z.Y., Tan, H.R., Tan, J.P.Y., Ng, S.C., Teo, E., 2012. Hydrothermal synthesis of CeO 2 nanocrystals: Ostwald ripening or oriented attachment?. Cryst. Growth Des. 12, 3296–3303. https://doi.org/10.1021/cg300421x.

Luo, Y., Zhang, W., Liao, Z., Yang, S., Yang, S., Li, X., et al., 2018. Role of Mn2+ doping in the preparation of core-shell structured Fe3O4@upconversion nanoparticles and their applications in T1/T2-weighted magnetic resonance imaging, upconversion luminescent imaging and near-infrared activated photodynamic therapy. Nanomaterials 8, 466. https://doi.org/10.3390/nano8070466.

Mehmood Ur Rehman, K., Liu, X., Li, M., Jiang, S., Wu, Y., Zhang, C., et al., 2017. Synthesization and magnetic properties of Ba1-xYxFe12O19 hexaferrites prepared by solid-state reaction method. J. M. Mag. Mat. 426, 183–187. https://doi.org/10.1016/j.jmmm.2016.10.001.

Mehmood Ur Rehman, K., Liu, X., Yang, Y., Feng, S., Tang, J., Ali, Z., et al., 2018. Structural, morphological and magnetic properties of Sr0.3La0.48Ca0.25n [Fe(2–0.4/n)O3]Co0.4 (n = 5.5, 5.6,5.7,5.8, 5.9, 6.0) hexaferrites prepared by facile ceramic route methodology. J. M. Mag. Mat. 449, 360–365. https://doi.org/10.1016/j.jmmm.2017.10.051.

Mehmood Ur Rehman, K., Riaz, M., Liu, X., Khan, M.W., Yang, Y., Batoo, K.M., et al., 2019. Magnetic properties of Ce doped M-type strontium hexaferrites synthesized by ceramic route. J. M. Mag. Mater. 474, 83–89. https://doi.org/10.1016/j.jmmm.2018.10.087.

Parvathya, S., Venkatramanb, B.R., 2017. In vitro antibacterial and anticancer potential of CeO_2 nanoparticles prepared by Co-precipitation and green synthesis method. Nanosci. Curr. Res. 2, 2.

Saikia, H., Hazarika, K.K., Chutia, B., Choudhury, B., Bharali, P., 2017. A Simple Chemical Route toward High Surface Area CeO_2 nanoparticles displaying remarkable radical scavenging activity. ChemistrySelect 2, 3369–3375. https://doi.org/10.1002/slct.201700354.

Saranya, J., Ranjith, K.S., Saravanan, P., Mangalaraj, D., Rajendra Kumar, R.T.R., 2014. Cobalt-doped cerium oxide nanoparticles: enhanced photocatalytic activity under UV and visible light irradiation. Mater. Sci. Semicond. Process. 26, 218–224. https://doi.org/10.1016/j.mssp.2014.03.054.

Syed Khadar, Y.A., Balamurugan, A., Devarajan, V.P., Subramanian, R., Dinesh Kumar, S., 2019. Synthesis, characterization and antibacterial activity of cobalt doped cerium oxide (CeO_2: Co) nanoparticles by using hydrothermal method. J. Mater. Res. Technol. 8, 267–274. https://doi.org/10.1016/j.jmrt.2017.12.005.

Watanabe, M., Yoneda, M., Morohashi, A., Hori, Y., Okamoto, D., Sato, A., et al., 2013. Effects of Fe3O4 magnetic nanoparticles on A549 cells. Int. J. Mol. Sci. 14, 15546–15560. https://doi.org/10.3390/ijms140815546.

Wojcieszak, D., Mazur, M., Kaczmarek, D., Domaradzki, J., 2018. Influence of doping with Co, Cu, Ce and Fe on structure and photocatalytic activity of TiO2 nanoparticles. Mater. Sci. Pol. 35, 725–732. https://doi.org/10.1515/msp-2017-0117.

Wu, Q., Zhang, F., Xiao, P., Tao, H., Wang, X., Hu, Z., 2008. Great influence of anions for controllable synthesis of CeO 2 nanostructures: from nanorods to nanocubes SI. J. Phys. Chem. C 112, 17076–17080. https://doi.org/10.1021/jp804140e.